RSC Applied Interfaces

ROYAL SOCIETY OF CHEMISTRY

PAPER

View Article Online
View Journal

Cite this: DOI: 10.1039/d6lf00080k

Benzoate-mediated generation of front–back reversible photoluminescence in transparent polymer/LDH:Tb,Eu nanocomposite films

Fumina Takahashi, Manabu Hagiwara and Shinobu Fujihara *

Transparent and luminescent organic/inorganic nanocomposite films were fabricated through aqueous solution routes. Water-soluble poly(vinyl alcohol) (PVA) was employed as an organic matrix, while hydrophilic layered double hydroxides (ZnAl-LDH) activated with rare-earth (RE) ions (Tb^{3+} or Eu^{3+}) were synthesized as flake-like nanoparticles to be used as inorganic luminescent components. Photoluminescence (PL) intensity could be increased by exchanging nitrate ions, which originated from raw materials and were initially included in ZnAl-LDH, for ultraviolet (UV)-absorbing benzoate ions through efficient energy transfer known as the antenna effect. A large difference in the wavelength-dependent absorbance of the benzoate ions was imprinted in the PL excitation spectra of our transparent films, opening an opportunity for controlling PL intensity based on the Lambert–Beer law. Such a PL mechanism was applied to multi-layer PVA/LDH:Tb,Eu nanocomposite films having unique emission properties including mixed-color emissions upon excitation at one wavelength, continuously and reversibly color-tunable emissions upon moving slowly, and distinctly color-switching emissions upon flipping over. Our results will be useful for designing and developing easily formable and highly flexible optical components necessary for directional UV imaging, security printing, fluorescence sensing, and so on.

Received 10th March 2026,
Accepted 13th May 2026

DOI: 10.1039/d6lf00080k

rsc.li/RSCApplInter

1. Introduction

Optical materials having a combination of light transmission and emission properties are promising for new applications in the field of energy, security, or agriculture in addition to common optics and optoelectronics.[1–5] For example, Shoji *et al.*[4] fabricated transparent and luminescent coating films of *ca.* 60 μm in thickness, consisting of Eu^{3+} complexes and tris(2,6-dimethoxyphenyl)phosphine oxide, on 100 μm thick, polyolefin-type polymer films. The resultant bi-layer films were used as greenhouse sheets for plant growth experiments. Significant promotion of the growth was observed for vegetal crops and trees because of the accumulated red-light emission from Eu^{3+} for enhancing the photosynthesis.

In many cases, transparent and luminescent materials are fabricated as coating or self-standing films for their practical use as introduced above. While inorganic films basically require substrates in both fabrication and utilization due to their mechanical hardness, organic or organic/inorganic films, as well as organic substrates, are flexible and are more versatile for large-area applications. A representative example of the latter is a transparent polymer film embedded with luminescent substances on the nanometer scale. Such substances are roughly classified into three groups: inorganic crystalline compounds with or without activators, fluorescent inorganic complexes or organic molecules, and surface-modified quantum dots. Each of them has both advantages and limitations due to their structural, physical, and chemical properties when dispersed in a polymer matrix. It is more favorable that the dispersoid has higher affinity with the dispersion medium for achieving better dispersibility. The choice of luminescent components, therefore, depends on the characteristics of the polymer such as the monomer structure, the chain structure, the molecular weight, and the distribution of functional groups.

The present study has also focused on the polymer matrix. Poly(vinyl alcohol) (PVA) was chosen due to its wide-range transparency, biocompatibility and biodegradability, and low gas permeability. In addition, its water-solubility is attractive in waste and recycling as well as in mass production. PVA has accordingly been used in various technological fields including drug delivery,[6] artificial tissues,[7] and food-packaging.[8] Both thermal and mechanical properties of PVA can be enhanced by adopting an organic/inorganic hybrid or composite structure.[9] Because PVA is a typical hydrophilic polymer due to the numerous OH groups in its structure, it has a high affinity to metal oxides and hydroxides through the hydrogen bond and the M–O–C (M: metal) bond.[10] Thus the design of luminescent

Department of Applied Chemistry, Faculty of Science and Technology, Keio University, 3-14-1 Hiyoshi, Kohoku-ku, Yokohama 223-8522, Japan.
E-mail: shinobu@applc.keio.ac.jp

components should be centered on the activation of metal oxides or hydroxides.

Layered double hydroxides (LDHs) may be promising as host materials for activators because they have been employed as inorganic components to improve the physical properties of PVA.[11–13] LDHs are expressed by a general formula of $\left[M_{1-x}M'_x(OH)_2\right]^{x+}\left[A^{n-}_{x/n}\right]\cdot mH_2O$ where M and M′ represent divalent and trivalent metal cations, respectively, and x values are normally ranging from 0.2 to 0.4.[14] In PVA/LDH composites, the hydrogen bond between OH groups of both PVA chains and LDH crystals works for improving the tensile strength and decreasing the rate of thermal decomposition as compared to pristine PVA. As long as the size of the LDH crystals is in the Rayleigh scattering regime, visible transmittance of the PVA/LDH composites will be kept high especially in the film form.[11]

LDHs can be composed of metal cations of various combinations including representative MgAl-LDH,[15] ZnAl-LDH,[16] and NiAl-LDH.[17] Rare-earth (RE) ions can also be incorporated into the metal hydroxide layers of LDHs as trivalent cations, which are expected to show photoluminescence (PL) under specific and managed conditions. In particular, the PL intensity of RE-doped LDHs is possibly increased by the intercalation of chemical species which can absorb shorter-wavelength light strongly and transfer the energy to RE ions.[18] This phenomenon is often called the antenna effect and has been utilized to design and synthesize RE complexes with much improved PL properties.

In the present work, ZnAl-LDH was doped with Tb^{3+} or Eu^{3+} ions and also was intercalated with benzoate ions. LDH nanoparticles were first synthesized as dried powders for the basic characterization of their structure and PL properties. Slurries of the LDH nanoparticles were then prepared to be mixed with PVA solutions for the film fabrication. Transparent and luminescent PVA/LDH nanocomposite films were formed on plastic substrates by using a film coating applicator. The PL properties of the nanocomposite films were significantly dependent on the absolute amount of the ultraviolet (UV)-absorbing benzoate ions present therein. This is due to the characteristic absorption spectrum of the phenyl group consisting of a few overlapping peaks with different intensities. Stacking of green- and red-emitting layers, as well as insertion of UV-absorbing and non-emitting layers, led to fine-tuning of the PL properties of the films. Because the films could be easily removed from the substrate, we have obtained a transparent material that shows front–back reversible emission colors. Optical systems using this type of material have been emerging very recently and are promising as, for example, short-wavelength imaging devices for visualizing X-rays or UV light and advanced displays enabling users to see front and back images in parallel.[19,20]

2. Experimental

2.1 Materials

All chemicals were of analytical grade and were used without further purification. $Zn(NO_3)_2\cdot 6H_2O$ (99.9%), $Al(NO_3)_3\cdot 9H_2O$ (99.9%), hexamethylenetetramine (HMT; 99.0%), and PVA with a degree of polymerization of 3100–3900 (86–90% hydrolyzed) were purchased from FUJIFILM Wako Pure Chemical Corporation, Japan. $Tb(NO_3)_3\cdot 6H_2O$ (99.95%), $Eu(NO_3)_3\cdot 6H_2O$ (99.95%), and sodium benzoate (SB; 98.0%) were purchased from Kanto Chemical Co., Inc., Japan. Polyethylene terephthalate (PET) films of 100 μm in thickness (Lumirror® T60, Toray Industries, Inc., Japan) were used as polymer substrates. Butene diol/vinyl alcohol copolymer (BVOH; Nichigo G-Polymer™, OKS-8118, Mitsubishi Chemical Corporation, Japan) was employed as a water-soluble and transparent dispersant.

2.2 Preparation of LDH components

ZnAlTb-LDH was synthesized by a homogeneous co-precipitation method. 4.00 mmol of $Zn(NO_3)_2\cdot 6H_2O$, 1.60 mmol of $Al(NO_3)_3\cdot 9H_2O$, and 0.400 mmol of $Tb(NO_3)_3\cdot 6H_2O$ were dissolved in 80 mL of deionized water. 10.4 mmol of HMT was further added to the solution, followed by stirring for 30 min and subsequent heating at 65 °C for 24 h. Formed precipitates were collected by being centrifuged and then were washed with deionized water three times to obtain the sample, designated as "LDH(N)Tb", in a slurry form. For characterization purposes, the slurry was dried at 65 °C for 24 h and the resulting solid matter was ground into a powder.

Benzoate-intercalated ZnAlTb-LDH was prepared by adding 10 mL of an aqueous SB solution (1.5 M) to the above-mentioned solution at the time just after heating at 65 °C for 24 h. The solution was then stirred for 1 h at room temperature. The precipitates were treated as above to obtain "LDH(B)Tb" both in the slurry and the powder form.

ZnAlEu-LDH was also synthesized similarly, where only the amount of $Al(NO_3)_3\cdot 9H_2O$ and $Eu(NO_3)_3\cdot 6H_2O$ was adjusted to 1.80 and 0.200 mmol, respectively. LDH(N)Eu and LDH(B)Eu were obtained as both a slurry and powder.

2.3 Fabrication of single-LDH nanocomposite films

The LDH slurry was further dispersed in deionized water to adjust its concentration to 20 wt%. An aqueous solution of 20 wt% BVOH, which was employed to suppress aggregation of the LDH nanoparticles, was prepared separately. 5 mL of the LDH(B)Tb or LDH(B)Eu slurry and 0.05 mL of the BVOH solution were added to 4.95 mL of deionized water, followed by stirring for 10 min and then sonication for 30 min. The aqueous LDH dispersion thus prepared was further mixed with 10 mL of an aqueous solution of 10 wt% PVA and was sonicated for 10 min to obtain a PVA/LDH(B)Tb or PVA/LDH(B)Eu coating solution.

PVA/LDH coating films of either LDH component were fabricated on the PET substrates, 105 × 150 mm^2 in size, by using a Smart Table Coater (TC-100S5, Mitsui Electric), attached with a variable applicator as a coating jig. The gap (denoted as d_{gap}) between the substrate surface and the coating blade was varied in the range of 100–1000 μm and was typically adjusted to 300 μm. The coating solution was placed on the substrate and was coated onto it with a speed

of 5 mm s^{-1}, followed by drying at 60 °C for 0.5 h. While the thickness of the freshly coated solution was close to d_{gap}, that of the dried film (denoted as d_{film}) decreased by more than 97%.

2.4 Fabrication of double-LDH nanocomposite films

Three series of PVA/LDH coating films were also fabricated using both LDH components at the same time. In one series, PVA/[(1 − x)LDH(B)Eu–xLDH(B)Tb] films (x series) were obtained from coating solutions containing both LDH components in molar ratios of LDH(B)Eu : LDH(B)Tb = (1 − x) : x, where x was varied between 0.1, 0.3, and 0.5. The film fabrication followed the above-mentioned process with d_{gap} = 300 μm.

In another series, the PVA/LDH(B)Eu film was coated first, followed by drying at 60 °C for 0.5 h, and then the PVA/LDH(B)Tb film was stacked on it to obtain bi-layer films. The thickness of each layer was adjusted by (1 − y) : y ratios, where y was varied between 0.1, 0.3, and 0.5. In the case of y = 0.1, for instance, the PVA/LDH(B)Eu and PVA/LDH(B)Tb films were coated sequentially with d_{gap} = 900 and 100 μm, respectively. Note that the total d_{gap} value was fixed at 1000 μm for all the (1 − y)[PVA/LDH(B)Eu]–y[PVA/LDH(B)Tb] films (y series).

In the other series, a PVA layer containing SB was further inserted between the above-mentioned two layers with y = 0.1. A coating solution for this middle layer was prepared by mixing 9 mL of an aqueous SB solution (0.1 M), 0.05 mL of the aqueous BVOH solution (20 wt%), 0.95 mL of deionized water, and 10 mL of the aqueous PVA solution (10 wt%). The bottom 0.9[PVA/LDH(B)Eu] layer was formed directly on the PET substrate through the coating (d_{gap} = 900 μm) and drying procedure. The middle z[PVA/SB] layer was similarly formed (d_{gap} = 100, 300, or 500 μm) on the pre-coated bottom layer. Finally, the top 0.1[PVA/LDH(B)Tb] layer was coated (d_{gap} = 100 μm) on the middle layer. The resultant triple-layer films were expressed as 0.9[PVA/LDH(B)Eu]–z[PVA/SB]–0.1[PVA/LDH(B)Tb] with z = 0.1, 0.3, or 0.5 (z series).

2.5 Characterization

The crystal structure of the LDH powders was identified with an X-ray diffractometer (D8 Advance, Bruker) using Cu Kα radiation. The chemical analysis of the powders was conducted with a Fourier transform infrared (FT-IR) spectrophotometer (Alpha, Bruker) using the KBr method. The particle morphology of the powders was observed with a field-emission transmission electron microscope (FETEM, Tecnai G2, FEI). Specimens for the observation were prepared by dispersing the LDH slurry in ethanol and then putting the particles onto a copper grid covered with a collodion film. The cross section of the PVA/LDH films was examined with another type of TEM (Tecnai, FEI). For the observation, the PET substrate coated with the PVA/LDH film was sliced into a few hundred nm thick specimen using an ultramicrotome.

The PL properties of the LDH powders and the PVA/LDH films were measured at room temperature with a spectrofluorometer (FP-8500, JASCO). The powder sample was placed on a quartz glass cell, while the film sample was mounted directly onto the equipment. A UV filter (UV-390) was used to remove stray light originating from the excitation light. The PL excitation spectra of some selected samples were analyzed by deconvolution using a data analysis software package, OriginPro (OriginLab, OriginLab Corporation). The optical transmittance spectra of the PET substrate and the PVA/LDH films were measured with a UV-visible spectrophotometer (V-670, JASCO). The film morphology was observed with a laser scanning confocal microscope (LSCM, VK-X1000, Keyence). The thickness of the PVA/LDH films was estimated from optical interference observed in their transmittance spectra or was determined by the LSCM observation. Note that all the films were cut into 20 × 20 mm^2 before each characterization.

3. Results and discussion

3.1 Luminescent LDH components

Fig. 1a compares the X-ray diffraction (XRD) patterns of the LDH powders, namely, LDH(N)Tb and LDH(B)Tb, before and after the intercalation of the benzoate ions. The pattern of the LDH(N)Tb powder is consistent with that reported for the nitrate-intercalated ZnAl-LDH (PDF No. 055-0193) having two strong (003) and (006) basal reflection peaks. The (003) peak is actually observed at 2θ = 9.93° and hence the interplanar spacing is calculated to be 8.90 Å for LDH(N)Tb. Additionally, there also appear broad and asymmetric (012) and (110) diffraction peaks at 2θ = 34° and 60°, respectively, which are attributed to the turbostratic structure of LDH.[21] In contrast, the pattern of the LDH(B)Tb powder exhibits differently (003), (006), (009), and (0012) basal reflection peaks that can be assigned to the benzoate-intercalated ZnAl-LDH.[22] The interlayer spacing is largely increased to 15.8 Å, calculated from the (003) peak at 2θ = 5.59°, due to the incorporation of the larger benzoate ions.[18] The position and shape of the (012) and (110) peaks are almost unchanged, which indicates that the intralayer metal–hydroxide structure can be maintained after the anion exchange.

The FETEM images of the LDH powders are shown in Fig. S1 to compare the particle morphology. Note that the metal hydroxide compounds are generally sensitive to the electron beam and hence they are deteriorated by radiation damage at higher acceleration voltages and/or in longer periods of observation time,[23] which is a reason for the unavoidably weak contrast of the images in Fig. S1. The LDH(N)Tb particles (Fig. S1a) exhibit a flake-like morphology with a nearly hexagonal shape approximately 50 nm in diameter. A selected area electron diffraction (SAED) pattern taken from one of the particles depicts hexagonally arranged spots, which confirms that the above-mentioned particles correspond to LDH with a rhombohedral crystal structure. The LDH(B)Tb particle (Fig. S1b) has a similar flake-like morphology. It seems that the present anion exchange procedure does not cause severe destruction of the particle structure because the metal hydroxide layers are preserved as mentioned above.

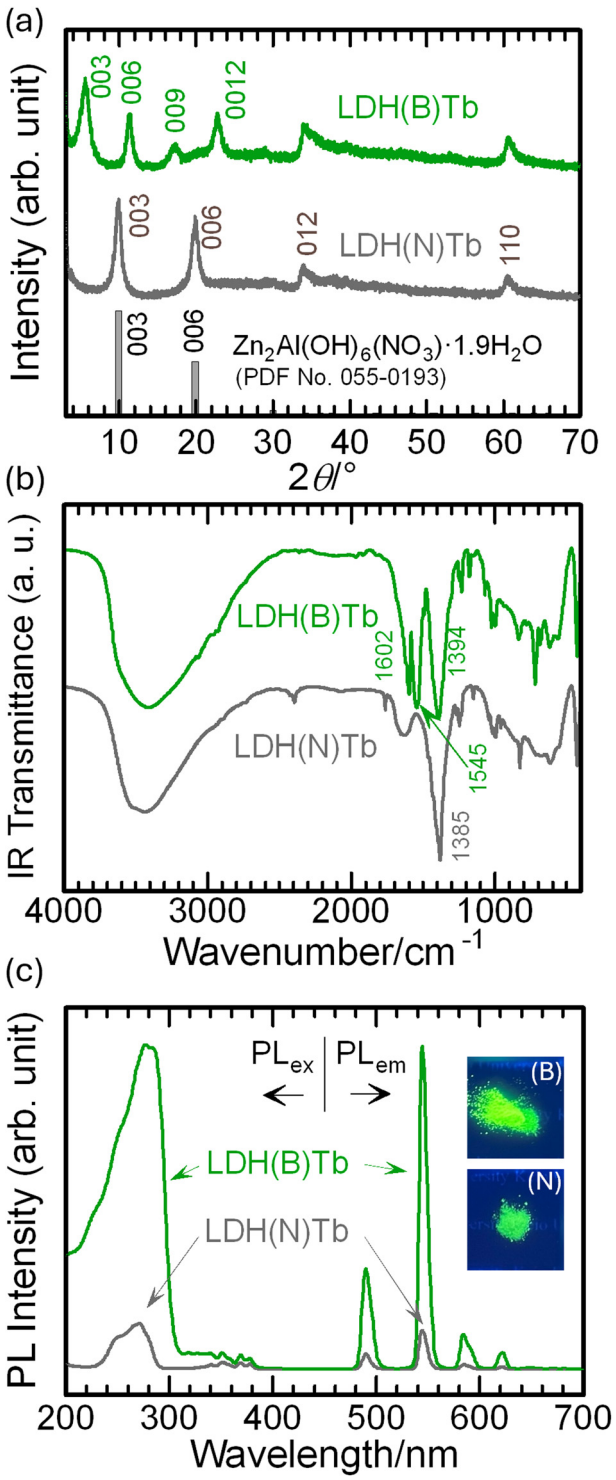

Fig. 1 (a) XRD patterns, (b) FT-IR spectra, and (c) PL_{ex} and PL_{em} spectra, together with photos under UV irradiation, of the LDH(N):Tb and LDH(B)Tb powders. The excitation wavelengths used for measuring PL_{em} were 270 and 278 nm for LDH(N):Tb and LDH(B)Tb, respectively.

The anionic species existing in the LDH powders were further analyzed by FT-IR to confirm the replacement of the nitrate with the benzoate ions. Fig. 1b shows the FT-IR spectra of the LDH powders before and after the anion exchange treatment. Both spectra have a broad absorption band peaking at around 3400 cm^{-1} due to the stretching vibration of the –OH groups of the hydroxide layers as well as the interlayer water molecules.[24] Individually, the LDH(N)Tb powder exhibits a strong absorption peak at around 1385 cm^{-1}, which is attributable to the stretching vibration of the nitrate ions.[25] The nitrate peak disappears in the LDH(B)Tb powder, and instead, the benzoate-related peaks are observed at 1602 cm^{-1} due to the skeletal vibration of the aromatic ring and at 1545 and 1394 cm^{-1} due to the antisymmetric and symmetric vibration of the COO^- groups, respectively.[22,26,27] The above FETEM and FT-IR results confirm that the anion exchange can be achieved without changing the morphology of the LDH particles on the nanometer scale.

The anion exchange led, as expected, to a change in the PL properties of the LDH powders. Fig. 1c shows the PL excitation (PL_{ex}) and emission (PL_{em}) spectra of the LDH(N)Tb and LDH(B)Tb powders. The inset photos were taken under irradiation with a 254 nm UV lamp. In the emission spectra, both LDH powders display sharp emission peaks centered at 490, 544, 585, and 622 nm that correspond to $^5D_4 \rightarrow {}^7F_{6,5,4,3}$ transitions of the Tb^{3+} ion.[28,29] Note that the PL intensity of the LDH(B)Tb powder excited at 278 nm is much larger than that of the LDH(N)Tb powder excited at 270 nm.

Two critical factors should be considered to interpret the PL properties of the present LDH powders. One is the appearance of a broad excitation band at wavelengths between 230 and 290 nm in the LDH(N)Tb powder. Such a band has not been observed in previous studies where the Tb^{3+}-doped, nitrate-intercalated LDH was synthesized by a co-precipitation method using ammonia or sodium hydroxide as the pH-adjusting agent.[30,31] In contrast, HMT was used to induce the homogeneous co-precipitation of LDH in the present experiment. This method is accompanied by the release of ammonia and formaldehyde, which might be further decomposed into ethanol, carbon dioxide, and water through self- as well as cross-disproportionation reactions.[32] A different experiment was conducted to examine the effect of HMT on the synthesis procedure of LDH(N)Tb. Firstly, LDH(N)Tb was prepared as a powder through the process described in the Experimental section. Secondly, the powder was dispersed in deionized water under stirring to try to wash out the impurities. Finally, the water-washed powder was treated with HMT by dispersing it in an aqueous HMT solution under stirring. Fig. S2a compares the PL_{ex} and PL_{em} spectra of the LDH(N)Tb samples thus obtained. The PL intensity is decreased by the water washing and is recovered by the HMT treatment. Fig. S2b shows a diffuse reflectance spectrum measured for the as-received HMT, wherein absorption peaks are observed at 226 and 272 nm. The longer-wavelength peak corresponds to the excitation peaks of the three LDH(N)Tb samples, thereby indicating the occurrence of UV absorption by HMT and subsequent energy transfer to the doped Tb^{3+} ions. Minor excitation peaks appearing in the spectrum between 340 and 390 nm come from the direct excitation of Tb^{3+} through 4f–4f electronic transitions.[33]

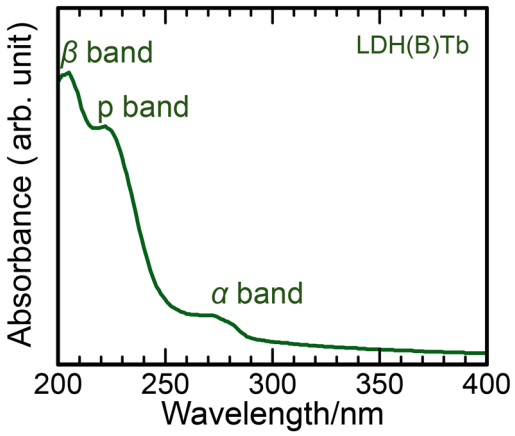

Fig. 2 An optical absorption spectrum of the diluted LDH(B)Tb slurry.

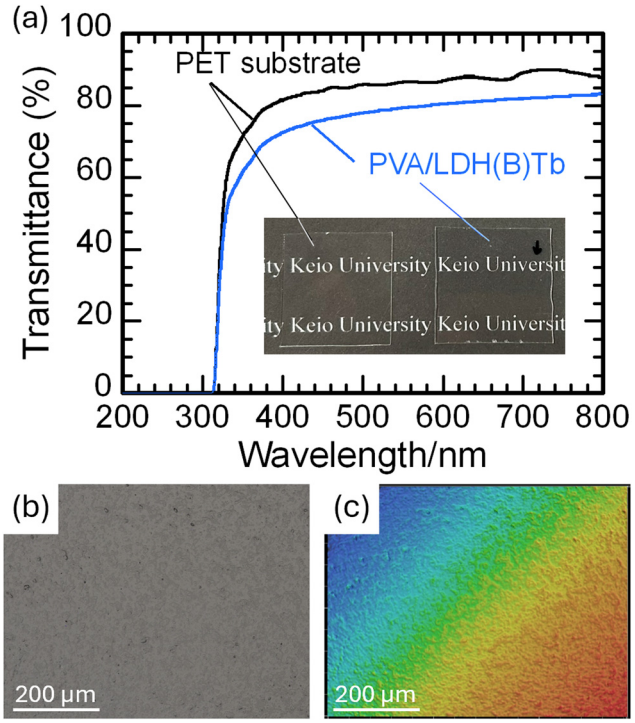

Fig. 3 (a) Optical transmittance spectra of the PET substrate and the PVA/LDH(B)Tb film together with their photos, and (b) an optical and (c) a two-dimensional LSCM image of the PVA/LDH(B)Tb film.

The other factor is the enhancement of the broad excitation band in the LDH(B)Tb powder, which should be related to the antenna effect through the benzoate ions. For confirmation, the LDH(B)Tb slurry was diluted to a concentration of 0.0025 wt% and its absorption spectrum was measured in the UV region. The result is shown in Fig. 2 where three main absorption bands appear at 271, 222, and 205 nm. These bands originate from π–π* transitions of the benzoate ions and are designated as α-, p-, and β-bands.[18] According to the Lambert–Beer law, the absorbance (A) of the benzoate ions is proportional to the molar absorption coefficient at the respective wavelengths (ε), the molar concentration (c), and the optical path length (l), and is expressed as follows:

$$A = \varepsilon c l \quad (1)$$

Assuming the absorbance and the coefficient for the α-, p-, and β-bands as A_α, A_p, and A_β, and ε_α, ε_p, and ε_β, the spectrum shown in Fig. 2 indicates their magnitude relationship as $A_\alpha < A_p < A_\beta$ that originates exclusively from the same relationship between the respective ε values, $\varepsilon_\alpha < \varepsilon_p < \varepsilon_\beta$. A comparison of the excitation spectrum in Fig. 1c and the absorption spectrum in Fig. 2 indicates that the efficient energy transfer occurs from the α- and p-bands to the 4f levels of the Tb^{3+} ions. LDH(B)Tb is therefore promising for use in transparent and luminescent hybrid films.

3.2 Luminescent PVA/LDH nanocomposite films

The slurry of LDH(B)Tb, referring again to the benzoate-intercalated ZnAlTb-LDH, was used to prepare the PVA/LDH nanocomposite films. Fig. 3a compares the optical characteristics of the PVA/LDH(B)Tb film and the bare PET substrate by showing their photos as well as optical transmittance spectra. The PET substrate is certainly transparent with transmittance of more than 80% in the entire visible light region. The absorption edge of PET is located at around 312 nm where transmittance is sharply decreased toward zero. After coating the PVA/LDH(B)Tb film, visible transmittance is slightly lowered due to scattering of the incident light. Because the PVA matrix alone does not influence the transparency of PET, as demonstrated in Fig. S3, the light scattering should be caused by the LDH(B)Tb nanoparticles. The appearance of the coated film is almost unchanged from the bare substrate, indicating that the present coating method is highly adaptable to the aqueous PVA solutions.

The smoothness of the film surface was also confirmed with the LSCM observation. A resulting optical micrograph in Fig. 3b shows that the film is free from the formation of cracks or voids, as well as the phase separation, throughout the coating procedure. Fig. 3c illustrates a two-dimensional LSCM image for the film surface shown in Fig. 3b. The appearance of color gradation, which corresponds to height distribution, is attributable to the curvature of the PET substrate, and no irregularities are detected from the coated film. The thickness of the film (d_{film}) was determined to be approximately 10 μm from the height of a step between the uncoated substrate and the coated edge. This d_{film} value is much smaller than d_{gap}, initially adjusted to 300 μm, due to the vaporization of the water solvent in the drying stage at 60 °C for 1 h. Although large shrinkage occurred in the depth direction, the film was free from wrinkles due to moderate drying conditions and the high flexibility of the polymer matrix.

The above-mentioned, 10 μm thick PVA/LDH(B)Tb film could be stripped off from the PET substrate using tweezers, allowing it to be handled like a self-standing, flexible polymer sheet. Fig. 4a shows a photo of the resulting transparent

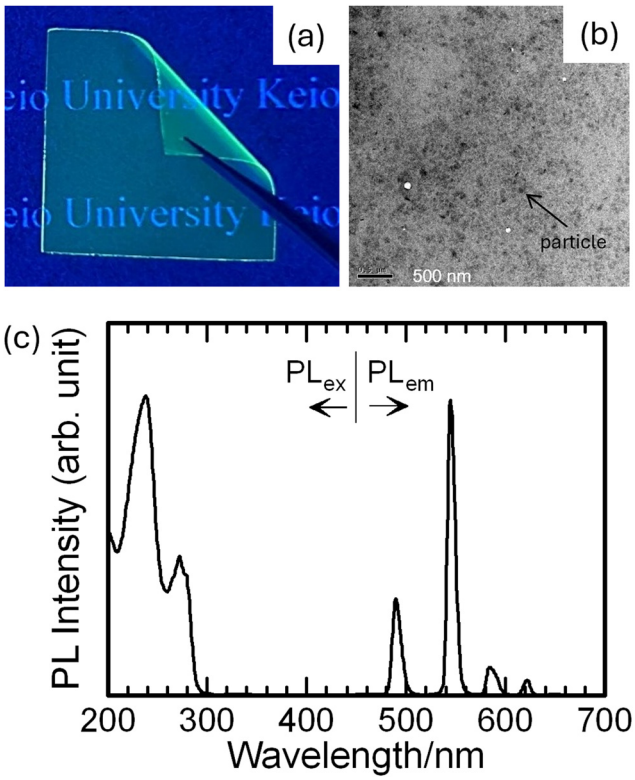

Fig. 4 (a) A photo of the self-standing PVA/LDH(B)Tb film under UV irradiation and (b) a cross-sectional TEM image and (c) PL_{ex} and PL_{em} spectra of the PVA/LDH(B)Tb film.

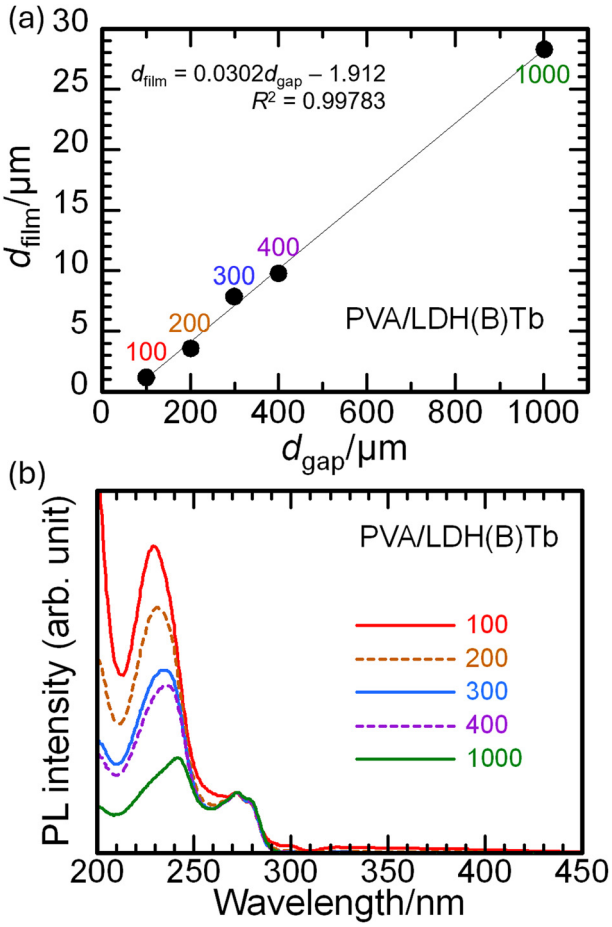

Fig. 5 (a) The relationship between d_{gap} and d_{film} and (b) PL_{ex} spectra for the PVA/LDH(B)Tb films fabricated with different d_{gap} values between 100 and 1000 μm.

sheet under irradiation with the 254 nm UV lamp. The sheet exhibits uniform green-light emission due to the inside luminescent LDH(B)Tb component. Cross-sectional TEM images taken from the film on the substrate (a few hundred nm thick) are shown in Fig. 4b and additionally in Fig. S4 with different magnifications. The one in Fig. 4b indicates that dark spots of approximately 50 nm in size are homogeneously dispersed throughout the cross section. The size corresponds to that of the LDH(B)Tb nanoparticles, which are more clearly seen in Fig. S4a than in Fig. S1b. A very small number of aggregated particles are observed in the image at low magnification (Fig. S4c). Fig. 4c shows the PL_{ex} and PL_{em} spectra of the film, as obtained under the common measurement conditions. When comparing Fig. 1c and 4c, the LDH(B)Tb powder and the PVA/LDH(B)Tb film exhibit similar PL_{em} spectra coming from the $^5D_4 \rightarrow {}^7F_{6,5,4,3}$ transitions of the Tb^{3+} ions.

By contrast, the PL_{ex} spectra of the two samples are different from each other in the apparent number of excitation bands and their relative intensity. Because the excitation process begins with the optical absorption of the benzoate ions, any difference might be caused by a change in their existing state. We experimentally confirmed that the PVA matrix did not affect the excitation behavior of the film and hence paid attention again to the absorption spectrum of the benzoate ions shown in Fig. 2. The absorbance also corresponds to the degree of the attenuation of the incident light. When the wavelengths fall into smaller absorbance and hence lower attenuation, the incident light is expected to reach farther in the benzoate-containing media. This should be a main reason for the different PL_{ex} spectra between the powder and the film and would generate the thickness-dependent PL_{ex} spectra in the PVA/LDH(B)Tb film.

The next issue was therefore to control the thickness (d_{film}) of the LDH(B)Tb films through varying the d_{gap} of the applicator in the coating process. The above experiment demonstrates that the d_{film}/d_{gap} ratio is around 0.03 under the condition of d_{gap} = 300 μm. Fig. 5a further verifies a linear d_{film}/d_{gap} relationship with a slope of 0.03 in the d_{gap} range between 100 and 1000 μm, which guarantees the high controllability of the present film-fabrication process.[34]

Fig. 5b compares the PL_{ex} spectra of the PVA/LDH(B)Tb films having different thicknesses. Note that each spectrum is normalized with the PL intensity at 272 nm, which is equivalent to the α-band in the absorption spectrum. A systematic change can be observed for the shape of the excitation spectra in accordance with the variation of the film thickness. That is, the excitation band ranging from 210 to 250 nm becomes relatively weaker as the thickness increases.

Moreover, the peak of this band shows a gradual shift to longer wavelengths.

Further analysis was made by comparing the PL_{ex} spectra of the LDH(B)Tb powder (Fig. 1c) and the thinner PVA/LDH(B)Tb film (d_{gap} = 300 μm) (Fig. 5b). Both spectra were subjected to baseline correction beforehand and were curve-fitted using the software package. Fig. 6 shows results in which each spectrum is deconvoluted into five peaks under the same fitting conditions. In comparison with the absorption spectrum of the diluted LDH(B)Tb slurry (Fig. 2), the PL_{ex} spectrum of the LDH(B)Tb powder is composed mainly of lower-absorbance components at longer wavelengths. On the other hand, the PVA/LDH(B)Tb film exhibits a PL_{ex} spectrum that highlights the two absorption bands, namely, the α- and p-bands, of the LDH(B)Tb slurry. As mentioned above, the attenuation of the incident light depends on the absorbance which is also proportional to the molar concentration and the optical path length. Because the abundance of the benzoate ions along the light path is much smaller in the PVA/LDH(B)Tb film than in the LDH(B)Tb powder, the p-band absorption can survive to provide the corresponding excitation peak in the former. When the film thickness is increased and hence the abundance of the benzoate ions becomes larger, the higher-absorbance components at the shorter wavelengths are attenuated gradually, as seen in Fig. 5b, and the spectrum should reach that of the powder as a final shape.

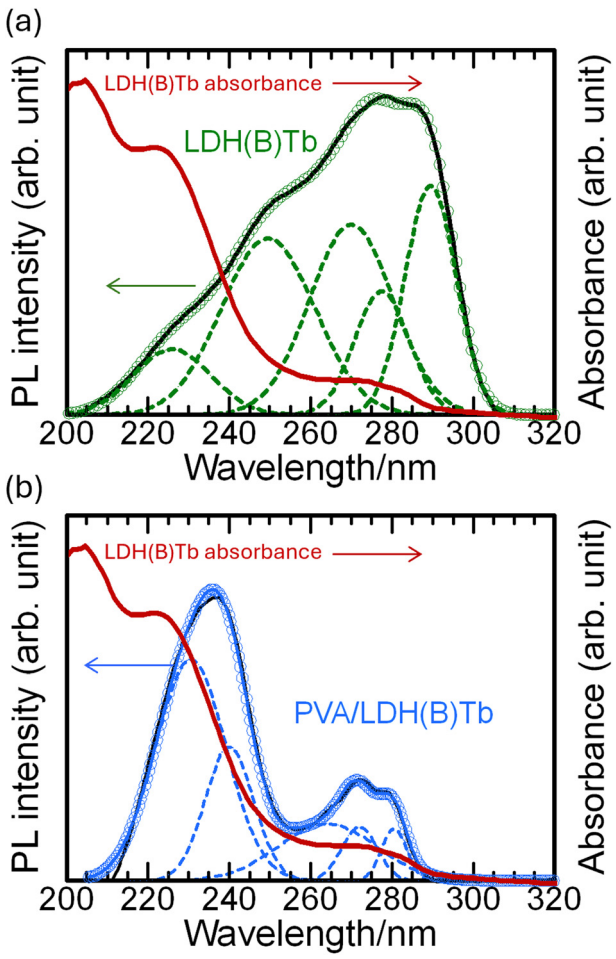

Fig. 6 The deconvoluted excitation spectra for (a) the LDH(B)Tb powder and (b) the PVA/LDH(B)Tb film with the smallest thickness. The absorption spectrum of the diluted LDH(B)Tb slurry is also shown as guidance.

3.3 Reversible luminescence of self-standing PVA/LDH films

For generating red luminescence concurrently, a similar fabrication process was adopted to the LDH(B)Eu powder and the PVA/LDH(B)Eu nanocomposite films. Fig. 7 shows the PL_{ex} and PL_{em} spectra of the resulting samples. In the PL_{em} spectra, both samples have the same emission behavior characteristic of the doped Eu^{3+} ions due to the $^5D_0 \rightarrow {}^7F_{1,2,3}$ transitions at 593, 614, and 651 nm. Among them, the hypersensitive electric-dipole $^5D_0 \rightarrow {}^7F_2$ transition gives the highest emission intensity, implying that the Eu^{3+} ions are basically located at a site without inversion symmetry. A comparison between Fig. 1c, 4c, and 7 makes it clear that the PVA/LDH(B)Tb and PVA/LDH(B)Eu films, as well as the LDH(B)Tb and LDH(B)Eu powders, have almost the same PL_{ex} spectra. This means that both Tb^{3+} and Eu^{3+} ions can be excited through the same mechanism which involves the optical absorption by the benzoate ions and the subsequent energy transfer to the Tb^{3+} or Eu^{3+} ions.

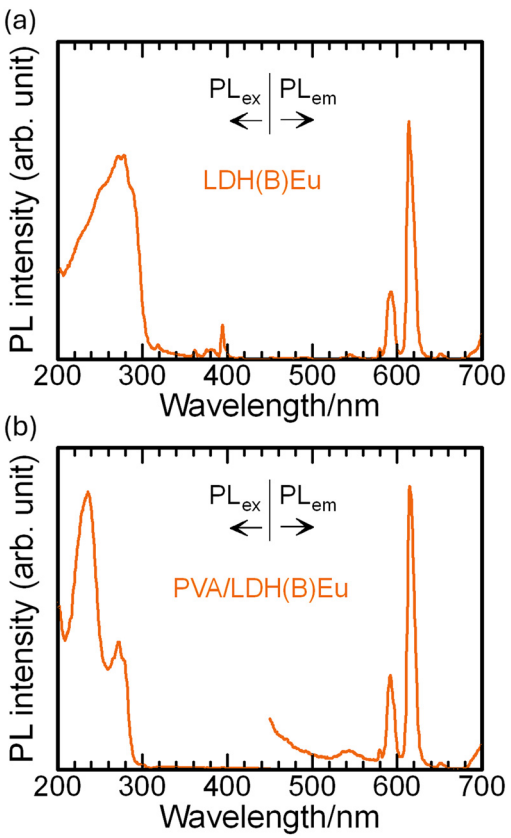

Fig. 7 PL_{ex} and PL_{em} spectra of (a) the LDH(B)Eu powder and (b) the PVA/LDH(B)Eu film.

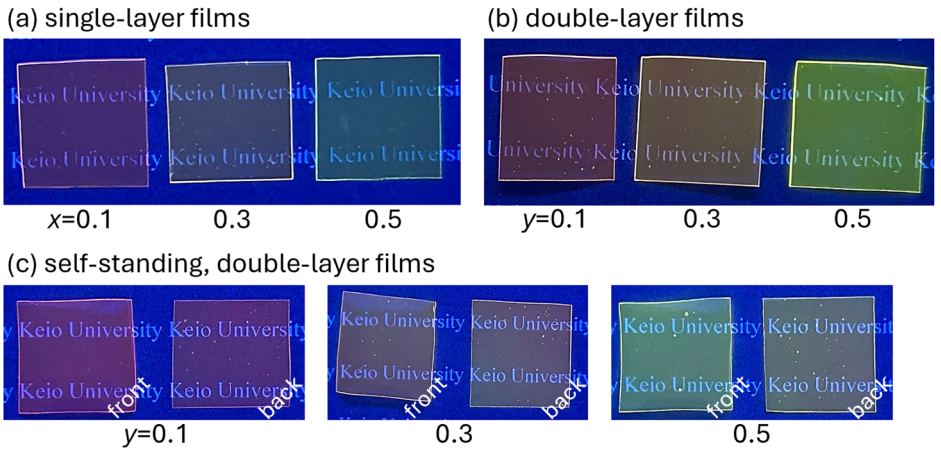

Fig. 8 Sample photos under UV irradiation: (a) the single-layer PVA/[(1 − *x*)LDH(B)Eu–*x*LDH(B)Tb] films, (b) the double-layer (1 − *y*)[PVA/LDH(B)Eu]–*y*[PVA/LDH(B)Tb] films, and (c) the front and back views of the double-layer films stripped off from the substrate.

The mixing effect of the Tb^{3+} and Eu^{3+} emissions was examined next using the single-layer (*x* series) and the double-layer (*y* series) nanocomposite films. In the *x*-series films, the nanoparticles of LDH(B)Eu and LDH(B)Tb would be dispersed randomly in the PVA matrix. Fig. 8a shows photos of the respective films under 254 nm UV irradiation. The PL emission is uniformly generated over the entire film surface and its color changes from red ($x = 0.1$) to yellow (0.3) or green (0.5) with a decrease in the proportion of LDH(B)Eu. More precise control of the emission color will be possible simply by adjusting the *x* value.

Also, the *y* value determines the LDH(B)Eu : LDH(B)Tb ratio in the film-thickness direction in the *y*-series films. A similar change in the emission color can therefore be seen with the variation of *y*, as shown in Fig. 8b, when irradiated with 254 nm UV light from the PVA/LDH(B)Tb side. It would then be interesting to observe the emission color from the PVA/LDH(B)Eu side, which was made possible by being stripped off from the PET substrate. Fig. 8c compares the emission color that is seen from both front and back sides in the respective self-standing films. The back-side emission appears to be slightly reddish at any *y*, indicating that the double-layer films can possibly have a reversible PL function. Generally, it has been difficult to create such a function in optically transparent materials such as glasses and polymers as well as coating films thereon.

A possible approach for the reversible PL can be deduced from the results and discussion presented above: (i) the PL emission of the RE ions doped in LDH is initiated by the antenna effect through the intercalated organic ions, (ii) the organic ions have several absorption bands of which the absorbance is largely different with each other, and (iii) the different absorbance can be effectively implemented in the transparent media. When the UV light enters the film vertically from one side, it undergoes attenuation as it propagates to the other side. The optical absorption by the benzoate ions should be a main cause of attenuation in the present case. As far as the Lambert–Beer law is adapted, the attenuation of the incident light is proportional to εcl. If we take d_{film} instead of l, the attenuation in the film is proportional to ε at fixed c and d_{film} and hence follows the relationship of $\varepsilon_\alpha < \varepsilon_p < \varepsilon_\beta$.

Fig. 9a presents the structure of the triple-layer nanocomposite films based on the above considerations. The top and bottom layers are the green-emitting PVA/LDH(B)Tb and red-emitting PVA/LDH(B)Eu films, respectively. The middle layer is newly inserted to control the excitation light and is composed of PVA and SB. Note that the $y = 0.1$ composition was chosen for the triple-layer films to maintain the red-emission intensity. The resultant triple-layer films were stripped off to be treated as self-standing films or, in other words, flexible sheets. Fig. 9b compares the transmittance spectra of the three transparent films ($z = 0.1$, 0.3, or 0.5) thus obtained. Visible-light transmittance increases slightly with increasing *z* value, which might be due to a decrease in light scattering. That is, as the thickness of the middle layer is increased during the coating and drying procedure, its uniformity is enhanced and accordingly its interface with the bottom and top layers becomes smoother. A photo of the film with $z = 0.5$ (Fig. 9c) presents the high transparency of the triple-layer nanocomposite film under indoor lighting.

Fig. 9b also proves that the UV absorption by the benzoate ions is intensified with the *z* value. This is simply because the number of the benzoate ions is multiplied along the light path as the thickness of the middle layer is expanded. Thus, the penetration distance of the UV excitation light can be tuned in the thickness direction of the triple-layer films. Photos shown in Fig. 9d and PL_{ex} and PL_{em} spectra collected in Fig. S5–S7 indicate clearly the effectiveness of the middle layer for changing the PL properties. Under UV irradiation from the front side, the films exhibit a remarkable color change from orange ($z = 0.1$) to green ($z = 0.5$). This implies that the excitation light can be blocked by the thicker middle layer for quenching the bottom layer. This works both ways: the films irradiated from the back side show a color change from orange ($z = 0.1$) to red ($z = 0.5$). Fig. 9e demonstrates

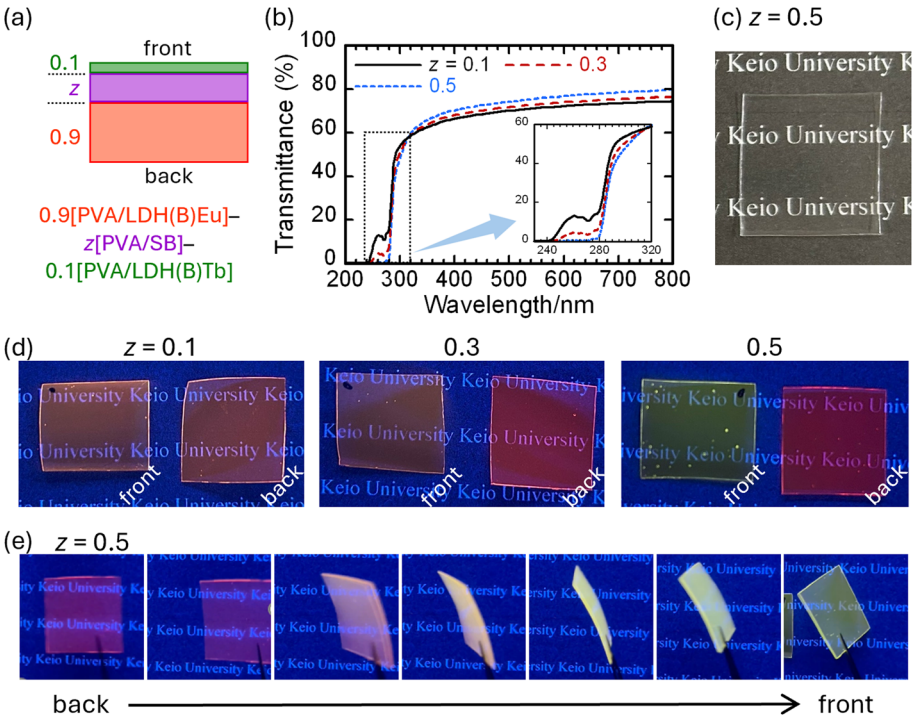

Fig. 9 (a) The schematic structure and (b) optical transmittance spectra of self-standing triple-layer nanocomposite films expressed as 0.9[PVA/LDH(B)Eu]–*z*[PVA/SB]–0.1[PVA/LDH(B)Tb] with an inset magnified view at wavelengths between 230 and 320 nm, (c) a photo of the film with z = 0.5 under indoor lighting, (d) photos of the films with z = 0.1, 0.3, or 0.5 taken from both front and back sides under the UV lamp, and (e) photos of the film with z = 0.5 while moving back to front under the UV lamp.

the way the film (z = 0.5) looks when it is turned over under UV light. Because the UV penetration depth changes complicatedly during this movement, there appears a variety of emission colors due to the mixing of the respective contributions from the PVA/LDH(B)Eu and PVA/LDH(B)Tb layers. As far as the antenna effect is involved in the excitation process, doping of other RE ions will help to expand the range of emission colors from the multi-layer PVA/LDH:RE nanocomposite films.

4. Conclusions

Transparent and luminescent organic/inorganic nanocomposite films consisting of a PVA matrix and benzoate-intercalated LDH:Tb,Eu nanoparticles were fabricated on PET substrates using a coating apparatus equipped with a thickness-controllable applicator. Under UV irradiation, the films exhibited PL emissions from the Tb^{3+} or Eu^{3+} ions doped in the LDH nanoparticles. The PL excitation was achieved by the antenna effect of the benzoate ions having three characteristic absorption bands. The different absorbance of these bands brought about variable intensity ratios of the excitation bands, depending on the thickness of the nanocomposite films. This result was applied to the fabrication of multi-layer films that were inserted with a UV-absorbing middle layer and hence could show front–back reversible PL features. Our results will be practically useful for developing new types of optical components such as directional UV imaging, security printing, fluorescence sensing, and so on.

Author contributions

Conceptualization: FT, SF; formal analysis: FT, MH; investigation: FT; methodology: FT, MH; resources: MH, SF; supervision: SF; visualization: FT, SF; writing – original draft: FT; writing – review and editing: SF.

Conflicts of interest

The authors declare no conflicts of interest regarding this study reported in the article.

Data availability

The authors confirm that the data supporting the findings of this study are available within the article and its supplementary information (SI).

Supplementary information: supporting TEM images, detailed spectral data, and additional experimental results. See DOI: https://doi.org/10.1039/d6lf00080k.

Notes and references

1 X. Huang, L. Zhang, S. Wang, D. Chi and S. J. Chua, *ACS Appl. Mater. Interfaces*, 2016, **8**, 15482–15488.
2 H. G. Jeon, H. Kim and S. H. Byeon, *Chem. Eng. J.*, 2021, **405**, 126675.
3 M. G. Debije and P. P. C. Verbunt, *Adv. Energy Mater.*, 2012, **2**, 12–35.

4 S. Shoji, H. Saito, Y. Jitsuyama, K. Tomita, Q. Haoyang, Y. Sakurai, Y. Okazaki, K. Aikawa, Y. Konishi, K. Sasaki, K. Fushimi, Y. Kitagawa, T. Suzuki and Y. Hasegawa, *Sci. Rep.*, 2022, **12**, 17155.
5 C. Zhuo, S. Zhao, X. Huang, Y. Jiang, J. Li and D. Fu, *J. Mol. Liq.*, 2023, **376**, 121442.
6 H. Jung, H. Kim and S. H. Byeon, *ACS Appl. Mater. Interfaces*, 2018, **10**, 43112–43121.
7 S. Jiang, S. Liu and W. Feng, *J. Mech. Behav. Biomed. Mater.*, 2011, **4**, 1228–1233.
8 J. Yu, C. Chen, J. B. Gilchrist, J.-C. Buffet, Z. Wu, C. Mo and D. O'Hare, *Mater. Horiz.*, 2021, **8**, 2823–2833.
9 F. Meng, Y. Zhang, Z. Xiong, G. Wang, F. Li and L. Zhang, *Composites, Part B*, 2018, **143**, 1–8.
10 G. Wu, Y. Yang, Y. Lei, D. Fu, Y. Y. Li, Y. Zhan, J. Zhen and M. Teng, *J. Coat. Technol. Res.*, 2020, **17**, 1145–1155.
11 S. Huang, X. Cen, H. Zhu, Z. Yang, W. W. Tjiu and T. Liu, *Mater. Chem. Phys.*, 2011, **130**, 890–896.
12 J. H. Yeun, G. S. Bang, B. J. Park, S. K. Ham and J. H. Chang, *J. Appl. Polym. Sci.*, 2006, **101**, 591–596.
13 K. Zhou, Z. Gui and Y. Hu, *Polym. Adv. Technol.*, 2017, **28**, 386–392.
14 Q. Wang and D. O'Hare, *Chem. Rev.*, 2012, **112**, 4124–4155.
15 M. Ogawa and H. Kaiho, *Langmuir*, 2002, **18**, 4240–4242.
16 F. Kooli, C. Depège, A. Ennaqadi, A. De Roy and J. P. Besse, *Clays Clay Miner.*, 1997, **45**, 92–98.
17 S. Kannan, A. Narayanan and C. S. Swamy, *J. Mater. Sci.*, 1996, **31**, 2353–2360.
18 X. Gao, M. Hu, L. Lei, D. O'Hare, C. Markland, Y. Sun and S. Faulkner, *Chem. Commun.*, 2011, **47**, 2104–2106.
19 X. Zhang, Y. Shi, X. Wang, Y. Liu and Y. Zhang, *ACS Nano*, 2022, **16**, 21576–21582.
20 L. Liu, X. Zhang, Z. Xia and Y. Zhang, *Sci. China Mater.*, 2026, **69**, 3222–3230.
21 A. V. Radha, P. V. Kamath and C. Shivakumara, *J. Phys. Chem. B*, 2007, **111**, 3411–3418.
22 P. Kovář, M. Pospíšil, M. Nocchetti, P. Čapková and K. Melánová, *J. Mol. Model.*, 2007, **13**, 937–942.
23 L. S. Gomez-Villalba, A. Sierra-Fernandez, M. E. Rabanal and R. Fort, *Ceram. Int.*, 2016, **42**, 9455–9466.
24 F. Kooli, I. C. Chisem, M. Vucelic and W. Jones, *Chem. Mater.*, 1996, **8**, 1969–1977.
25 Z. Karami, M. Jouyandeh, J. A. Ali, M. R. Ganjali, M. Aghazadeh, S. M. R. Paran, G. Naderi, D. Puglia and M. R. Saeb, *Prog. Org. Coat.*, 2019, **136**, 105218.
26 Y. Wang and D. Zhang, *Mater. Res. Bull.*, 2011, **46**, 1963–1968.
27 K. Saito, T. Xu and H. Ishikita, *J. Phys. Chem. B*, 2022, **126**, 4999–5006.
28 K. Sakuma and S. Fujihara, *J. Ceram. Process. Res.*, 2013, **14**, 26–29.
29 R. Sasai, K. Ohta, K. Makishima, T. Fujimura, C. Moriyoshi, J. Kumagai and S. Kawauchi, *Luminescence*, 2025, **40**, e70174.
30 Y. Chen, Y. Bao, G. Yang and Z. Yu, *Mater. Chem. Phys.*, 2016, **176**, 24–31.
31 I. Yanase, Y. Horiuchi and H. Kobayashi, *Mater. Res. Bull.*, 2019, **110**, 207–213.
32 S. Morooka, C. Wakai, N. Matubayasi and M. Nakahara, *J. Phys. Chem. A*, 2005, **109**, 6610–6619.
33 L. H. Zhang, Y. L. Li, Y. B. Zhou and C. Y. Zhang, *J. Appl. Spectrosc.*, 2022, **89**, 803–808.
34 An upper limit of d_{gap} is 5 mm in the present variable applicator. However, we confirmed that the constant d_{film}/d_{gap} ratio of around 0.03 was valid only at d_{gap} = 1000 μm or below. The d_{film} values became smaller than expected when adopting the larger d_{gap} values: for example, d_{film} was as small as 40 μm against d_{gap} = 4000 μm. It might be better to repeat the coating procedure to obtain thicker films.